sustainability

MDPI

Article

Effects of Autogenous and Stimulated Self-Healing on Durability and Mechanical Performance of UHPFRC: Validation of Tailored Test Method through Multi-Performance Healing-Induced Recovery Indices

Estefanía Cuenca, Francesco Lo Monte, Marina Moro, Andrea Schiona and Liberato Ferrara *

Department of Civil and Environmental Engineering, Politecnico di Milano, 20133 Milan, Italy; estefania.cuenca@polimi.it (E.C.); francesco.lo@polimi.it (F.L.M.); marina.moro@mail.polimi.it (M.M.); andrea.schiona@mail.polimi.it (A.S.)

* Correspondence: liberato.ferrara@polimi.it

Abstract: Chloride diffusion and penetration, and consequently chloride-induced corrosion of reinforcement, are among the most common mechanisms of deterioration of concrete structures, and, as such, the most widely and deeply investigated as well. The benefits of using Ultra-High Performance (Fiber-Reinforced) Concrete—UHP(FR)C to extend the service life of concrete structures in "chloride attack" scenarios have been addressed, mainly focusing on higher "intrinsic" durability of the aforementioned category of materials due to their compact microstructure. Scant, if nil, information exists on the chloride diffusion and penetration resistance of UHPC in the cracked state, which would be of the utmost importance, also considering the peculiar (tensile) behavior of the material and its high inborn autogenous healing capacity. On the other hand, studies aimed at quantifying the delay in chloride penetration promoted by self-healing, both autogenous and autonomous, of cracked (ordinary) concrete have started being promoted, further highlighting the need to investigate the multidirectional features of the phenomenon, in the direction both parallel and orthogonal to cracks. In this paper, a tailored experimental methodology is presented and validated to measure, with reference to its multidirectional features, the chloride penetration in cracked UHPC and the effects on it of self-healing, both autogenous and stimulated via crystalline admixtures. The methodology is based on micro-core drilling in different positions and at different depths of UHPC disks cracked in splitting and submitted to different exposure/healing times in a 33 g/L NaCl aqueous solution. Its validation is completed through comparison with visual image analysis of crack sealing on the same specimens as well as with the assessment of crack sealing and of mechanical and permeability healing-induced recovery performed, as previously validated by the authors, on companion specimens.

Keywords: self-healing; crystalline admixtures; chloride diffusion; ultra-high durability concrete

Citation: Cuenca, E.; Lo Monte, F.; Moro, M.; Schiona, A.; Ferrara, L. Effects of Autogenous and Stimulated Self-Healing on Durability and Mechanical Performance of UHPFRC: Validation of Tailored Test Method through Multi-Performance Healing-Induced Recovery Indices. *Sustainability* **2021**, *13*, 11386. https://doi.org/10.3390/su132011386

Academic Editor: Rui Micaelo

Received: 31 August 2021
Accepted: 7 October 2021
Published: 15 October 2021

1. Introduction

Self-healing concretes and self-healing technologies have nowadays reached quite a remarkable scientific maturity and technological readiness level and can surely represent a breakthrough innovation in the concrete construction industry and market to design and build more durable and longer-lasting structures and infrastructures.

Though their application is somewhat scattered, most often driven, meritoriously, by university–industry partnerships owners and/or investigators of each single technology, an agreed upon framework is so far lacking, mainly with reference to standardized test methodologies which should enable designers, contractors, and end-users to quantitatively assess the efficiency of a particular technology with reference to the performance demand of the intended application. State-of-the-art review papers have been published in an

attempt not only to make order among the paper disseminated information but also to address the research in the sight of the most crucial needs highlighted by the industry [1,2].

What is still missing, though some embryonic attempts can be found in the literature, is the formulation and validation of an approach which could enable to quantify the benefits of self-healing, by means of reliably and robustly measurable parameters, for which test standardization is essential, and incorporate them into numerical models [3,4] and durability-based design approaches [5], to be formulated and validated as well. This will continue to support a wider and wider market acceptance of self-healing technologies and will discard the misunderstood concept which regards self-healing as a mere bonus in civil structure and infrastructure engineering applications.

The same happens, e.g., for the durability of ultra-high-performance (fiber-reinforced) concrete (UHPC/UHPFRC) which, having been in most cases inferred, from an "educated guess", as an obvious consequence of the high compactness and extremely low porosity of the material, has more rarely been demonstrated in wider real structural service scenarios, which, as a matter of fact, do include cracked state of the material [6].

What only recently has also been agreed upon by the scientific and engineering community is the clear definition of the material set of performances whose healing-induced recovery has to be sought, achieved, and measured. In fact, in the largely abundant literature on the topic, healing is assessed, besides through visual evidence of crack closure, appropriately referred to as crack self-sealing, through the recovery, upon crack sealing itself, of durability related parameters, including, e.g., water capillary absorption, water permeability and, to a minor extent, chloride diffusion/penetration. Reduced values of the aforementioned parameters result in slower penetration of aggressive agents into concrete, with, e.g., delayed onset of reinforcement corrosion and hence slower degradation of the structural performance, which may ultimately result in longer structure service life. It is worth remarking that only recently approaches harmonizing the so-far garnered knowledge in this perspective have started being formulated and validated [5,7].

With specific reference to chloride penetration resistance, which has to be regarded as one of the most prominent durability performance of cement-based materials, also in the sight of enforcing a true performance-based durability design of reinforced concrete structures, an increasing number of studies have started addressing in the last year the topic with specific reference to the benefits which may be brought by the concrete self-healing capacity.

Autogenous healing of both ordinary concrete and mortars [8–15] was studied, together with stimulating effects of different supplementary cementitious materials [16,17] and crystalline admixtures [18–20] as well as the case of autonomous healing via bacteria [21] or polyurethane-based healing agent encapsulated into glass capsules [22,23], or through crack control via fibers [24].

Effectiveness of crack self-sealing, however produced, in delaying the chloride penetration was reliably assessed and confirmed [25], though a quantitative approach able to provide, e.g., a crack width-exposure time scenario dependent on the rate of recovery of chloride imperviousness, is far from being reached. This can be ascribed to the sparsity and variety of the database, to which even data mining strategies would hardly be applicable [26].

The approaches found in the literature are surely consistent for ordinary reinforced concrete structures, where tension (cracked) concrete is meant only to provide protection to the reinforcement against the penetration of aggressive agents, but can be limiting in the case of advanced cement-based materials, such as UHPC/UHPFRCs cited above.

On the one hand, the higher intrinsic durability of UHPC may lead to values of measured durability parameters which may fall within the sensitivity ranges of the same tests employed to measure them [27]. On the other hand, the signature tensile behavior of this category of cement-based materials is, as well known, characterized, in the service state, by the ability to spread an otherwise localized damage (crack) into a series of thinly opened and tightly spaced multiple cracks.

The inborn self-healing conduciveness of a narrow crack, as compared to a wider one, is in this category of materials further enhanced by the peculiar mix composition, which is designed to achieve the aforementioned behavior [28–30]. This composition features high cement and binder content and low water/binder ratios, thus providing ample resources for delayed hydration of anhydrous particles exposed to water and/or outdoor moisture upon cracking.

Furthermore, it is worth remarking that the stable multiple cracking behavior is made possible by the peculiar mix compositions, designed through a micromechanically based approach that balances crack tip toughness and fiber pull-out energy. This results in a strain-hardening tensile behavior which, with its constitutive parameters, enters explicitly into the structural design of structures made of, or retrofitted with, this category of advanced cement-based materials [31].

In this respect, the assessment of the healing-induced recovery of the material has to encompass both the durability/transport properties and the mechanical ones, the healing-related recovery of the latter being likewise responsible, together with the former one, of the stability over time of the structural performance in the intended scenario, with is the truest and broadest meaning of structural durability. This also brings the breakthrough concept of transforming the material from a passive provider of protection into an active player, able to respond to degradation processes as a function of the durability requirements of the engineering application [32]. In this framework, it is evident that the experimental methodology conceived to assess the self-healing capacity of this category of materials has to be soundly based on a multiplicity of tests [33], enabling the quantification of the closure of the cracks as well as the recovery of the durability properties, which surely relies on the former, and of their mechanical tensile properties, which benefit not only from the reconstruction of the through-crack material continuity but also from a healing-induced enhancement of the fiber–matrix bond.

In this paper, the proposal for such a methodology, based on chloride diffusion tests complemented with mechanical tests and water permeability tests and visual crack inspection, is illustrated and validated with reference to autogenous and crystalline admixture-stimulated healing performance of a UHPC/UHPFRC healed up to one year in chloride solution/water immersion.

The material employed has been designed and tested, with reference to its mechanical and durability performance [27,31–33], to be employed for the construction of a tank containing geothermal water and serving cooling towers in a geothermal power plant, as a pilot demonstrator of the Horizon 2020 ReSHEALience project (rethinking coastal defense and green-energy service infrastructures through enHancEd-durAbiLity high-performance cement-based materials-GA 780624—www.uhdc.eu, accessed on 6 October 2021) [5,32].

With specific reference to chloride penetration resistance, it has been evaluated on disk specimens, both un-cracked and pre-cracked via splitting tests and upon immersion up to six months in a 33 g/L NaCl aqueous solution, by micro-core drilling at different positions parallel to the diameter crack length, at different distances orthogonal from the crack plane, and at different depths parallel to the crack depth. Chemical titration of the drilled material allowed to obtain chloride content across a 3D matrix consisting of thirty-six evaluation points for each specimen, thus enabling the reconstruction of the chloride penetration profile both along the crack depth and length and orthogonal to it.

Comparison with healing-induced recovery of water permeability and mechanical flexural performance (in terms of both stiffness and load-bearing capacity) as well as with image analysis quantification of crack sealing paves the way for the definition of a crack width and exposure time-dependent performance recovery relationship.

The methodology, for which this paper will present a thorough validation, and the material herein proposed have been also selected for a round-robin test, which, besides involving the laboratories of the university partners of the ReSHEALience project (Universitat Politecnica de Valencia, Spain; Institute of Construction Science Eduardo Torroja, CSIC, Madrid; Institute of Construction Materials, Technische Universiteit Dresden, Ger-

many; Faculty for the Built Environment, University of Malta) has also been extended, in a synergic effect, to four other partners of the COST Action CA1502 SARCOS (Self-healing As prevention Repair of COncrete Structures—www.sarcos.eng.cam.ac.uk/, accessed on 6 October 2021) (University of Minho, Guimaraes, Portugal; University of Loughborough, UK; University of Gent, Belgium).

The tailored analysis of the whole set of data garnered through this activity is the subject of another dedicated paper and will also form the basis for further investigation and validation in the framework of the MSCA-ITN SMARTINCS (Self-Healing, Multifunction, Advanced Repair Technologies in Cementitious Systems-GA 860006—www.smartincs.ugent.be, accessed on 6 October 2021).

2. Experimental Methodology

2.1. Materials and Mix Design Proportions

The experimental program has been designed focusing on a UHPC/UHPFRC, whose composition is detailed in Table 1, with a water/cement ratio equal to 0.33 and a water/binder ratio equal to 0.18. The low water/cement and water/binder ratio, together with the high content of the binder, is highly conducive to autogenous crack-sealing and self-healing capacity. Stimulation of this capacity was also performed in this study, through the addition of crystalline admixture (Penetron Admix®), dosed at 0.8% of cement weight. Its morphological and chemical characteristics have been already described in [34–36].

Table 1. Mix design of the employed UHPC/UHPFRC.

Constituents [kg/m^3]	without (w/o) CA	with (w) CA
Cement CEM I 52.5R	600	
Slag	500	
Water	200	
Steel fibers Azichem Readymix 200®	120	
Sand (0–2 mm)	982	
Superplasticizer BASF Glenium ACE 300®	33	
Crystalline admixtures (CA) Penetron Admix®	0	4.8

Table 2 reports the chemical composition of the employed cement and slag and Table 3 details the mixing protocol followed to produce the concretes.

Table 2. Chemical composition of the employed cement and slag. (LOI: loss on ignition @1000 °C).

Oxide wt.%	CaO	SiO_2	Al_2O_3	MgO	SO_3	Fe_2O_3	TiO_2	Mn_2O_3/MnO	K_2O	Na_2O	Other	LOI
PC	59.7	19.5	4.9	3.3	3.4	3.5	0.2	0.1	0.8	0.2	0.4	2.5
BFS	39.2	38.9	10.2	6.4	1.3	0.4	0.6	0.3	0.5	0.8	0.3	1.2

Table 3. Mixing protocol.

Mixing Order	Step	Mixing Time (min)
1	Dry mixing of cement, slag, sand, and CA (if present)	0–2
2	Add water	2–3
3	Add superplasticizer	3–5
4	High-speed mixing	5–11
5	Add steel fibers	11–16
6	High-speed mixing	16–26

This was calibrated to obtain a self-leveling consistency and guarantee a proper dispersion of the steel fibers (l_f = 20 mm; d_f = 0.22 mm), which were added at a volume fraction equal to 1.5% in order to obtain a strain-hardening tensile response at the required level of strength and deformation capacity [31]. The objective of the whole experimental

program was to characterize, through a tailored experimental methodology, the self-healing capacity in HPFRCC with and without crystalline admixtures.

2.2. Tests and Analysis Methods

Because of its high matrix compactness, which prevents and delays the ingress and transport of aggressive substances, UHPC/UHPFRC has an intrinsic high durability in the un-cracked state [27]. On the other hand, it is usually designed in order to have a strain-hardening behavior in bending and/or even in direct tension, this behavior allowing the formation of several small cracks which may be favorable for a faster and higher effectiveness of self-healing processes [26,37].

The synergy between an otherwise localized damage spread into multiple tiny cracks and the autogenous or stimulated capacity of the material to heal them—in case also upon repeated consecutive cracking events—has been regarded as a key aspect to address the durability. In particular, reference is made to the, so far not frequently investigated, durability of this category of cementitious composites in the cracked state, which, it is worth remarking, represents the real structural service scenario for advanced cement-based materials as well.

This is of paramount importance if code acceptance/incorporation of these same materials has to be sought and pursued, most of all with the aim of developing a durability-based structural design approach. These would mean overcoming the—often automatically satisfied—currently holding prescriptive composition requirements, by preferring a performance-based approach. Hence, starting from the identification of the value of performance parameters governing the degradation-related transport phenomena, their effects should be assessed on the persistence of the mechanical and structural performance.

In this framework, the testing strategy adopted for the assessment of the self-healing capacity of the investigated mixes was conceived in order to provide an as broad as possible response to the aforementioned issue. In the following, three tests are proposed:

(1) evaluation of self-healing through evolution of chlorides diffusion in pre-cracked disks (Section 2.2.1);
(2) evaluation of self-healing through recovery of water permeability in pre-cracked disks (Section 2.2.2);
(3) evaluation of self-healing through recovery of mechanical performance in thin beams tested in four-point bending (Section 2.2.3).

Before testing, all the samples were cured in a moist room or immersed in tap water as indicated in Table 4 for 60 days. The same samples have been tested before pre-cracking (for water permeability and chloride diffusion), before healing (time 0, namely just after pre-cracking), and after the three scheduled healing periods, equal to one, three, and six months (twelve for mechanical tests).

Table 4. Experimental program for bending tests on thin beams.

Specimen ID	Exposure Condition	Month 0		Month 1		Month 3		Month 12	
		Test	ε_{tot} [‰]	Test	ε_{tot} [‰]	Test	ε_{tot} [‰]	Test	ε_{tot} [‰]
w/o CA 1-1	Immersion	Pre-crack	1	Re-crack	2	Re-crack	3	Re-crack	4
w/o CA 1-2	Moist rm	-	-	-	-	Failure	-	-	-
w/o CA 1-3	Immersion	Pre-crack	1	Re-crack	2	Re-crack	3	Re-crack	4
w/o CA 1-4	Moist rm	Failure	-	-	-	-	-	-	-
w/o CA 1-5	Immersion	Pre-crack	1	Re-crack	2	Re-crack	3	Re-crack	4
w/o CA 1-6	Moist rm	-	-	-	-	-	-	Failure	-
w/o CA 1-7	Moist rm	-	-	-	-	Failure	-	-	-
w/o CA 1-8	Immersion	Pre-crack	1	Re-crack	2	Re-crack	3	Re-crack	4
w/o CA 1-9	Moist rm	Failure	-	-	-	-	-	-	-
w/o CA1-10	Immersion	Pre-crack	1	Re-crack	2	Re-crack	3	Re-crack	4
w/o CA 2-1	Immersion	Pre-crack	1	Re-crack	2	Re-crack	3	Re-crack	4
w/o CA 2-2	Moist rm	-	-	Failure	-	-	-	-	-
w/o CA 2-3	Immersion	Pre-crack	1	Re-crack	2	Re-crack	3	Re-crack	4
w/o CA 2-6	Moist rm	-	-	-	-	-	-	Failure	-
w/o CA 2-7	Moist rm	-	-	Failure	-	-	-	-	-
w CA 1-1	Moist rm	-	-	-	-	Failure	-	-	-
w CA 1-2	Immersion	Pre-crack	1	Re-crack	2	Re-crack	3	Re-crack	4
w CA 1-3	Immersion	Pre-crack	1	Re-crack	2	Re-crack	3	Re-crack	4
w CA 1-4	Moist rm	Failure	-	-	-	-	-	-	-
w CA 1-5	Immersion	Pre-crack	1	Re-crack	2	Re-crack	3	Re-crack	4
w CA 1-6	Immersion	Pre-crack	1	Re-crack	2	Re-crack	3	Re-crack	4
w CA 1-7	Moist rm	-	-	-	-	Failure	-	-	-
w CA 1-8	Immersion	Pre-crack	1	Re-crack	2	Re-crack	3	Re-crack	4
w CA 1-9	Moist rm	Failure	-	-	-	-	-	-	-
w CA1-10	Immersion	Pre-crack	1	Re-crack	2	Re-crack	3	Re-crack	4
w CA 2-1	Moist rm	-	-	-	-	-	-	Failure	-
w CA 2-2	Moist rm	-	-	Failure	-	-	-	-	-
w CA 2-3	Immersion	Pre-crack	1	Re-crack	2	Re-crack	3	Re-crack	4
w CA 2-6	Moist rm	-	-	-	-	-	-	Failure	-
w CA 2-7	Moist rm	-	-	Failure	-	-	-	-	-

After the pre-cracking and before performing the tests at scheduled healing times, all the cracks were visually inspected via a microscope as it will be detailed hereafter to quantify the crack sealing.

2.2.1. Self-Healing Assessment through Evolution of Chlorides Penetration

Concrete disks Ø100 × 80 mm were obtained by cutting concrete cylinders Ø100 × 280 mm after having discarded the ends. For each mix, a total of nine disks were obtained from the three cylinders devoted to the chloride penetration test.

Six out of the nine concrete disks were pre-cracked by splitting test up to a residual crack width of 100 ± 50 µm after unloading. Displacement transducers were placed on the disk for monitoring the crack width during the splitting test (Figure 1).

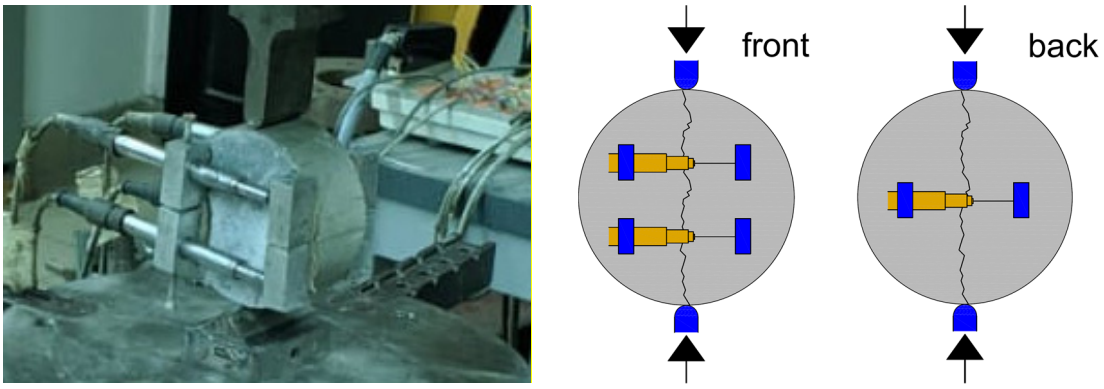

Figure 1. Pre-cracking of disk specimens by means of crack-opening controlled splitting test (with front and rear view of the set-up).

All the samples were then waterproofed with silicone and tape on the lateral surface and on one of the two bases, in order to enforce a unidimensional inlet of water.

The specimens were then immersed in water with 33 g/L of NaCl (in order to simulate an environment similar to seawater) for their healing, changing the curing bath every month.

After pre-cracking and at the target time, specimens were taken out of the chloride solution and cracks were analyzed via an image processing protocol as follows.

At least three microscope images were taken for each diameter crack at equidistant points of the length of the crack at each of the two faces of the specimen. The average crack width was calculated. Images were then processed via image processing software Photoshop® (see Figure 2), to reconstruct the crack as a whole, and then converted into a set of black pixels and so quantifying its area as a function of curing time. Hence, the *Index of Crack Sealing* (*ICS*) was computed as follows:

$$ICS = 1 - \frac{A_i}{A_{i-1}} \cdot \frac{L_{i-1}}{L_i} = 1 - \frac{w_i}{w_{i-1}} \quad (1)$$

where A_{i-1} is the crack area just after re-cracking, A_i is the crack area at the end of the healing period, L_{i-1} is the crack length just after re-cracking, L_i is the crack length at the end of the healing period, w_{i-1} is the average crack width just after re-cracking, and w_i is the average crack width at the end of the healing period.

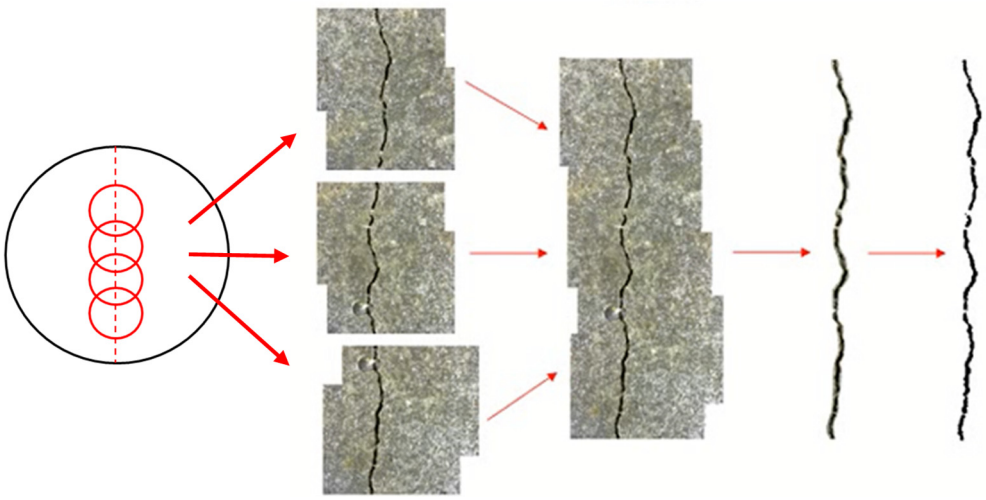

Figure 2. Image processing procedure for microscope image analysis of cracks and determination of the index of crack sealing (ICS).

The determination of chloride penetration depth through $AgNO_3$ sprayed on the cracked surfaces provided somewhat inconsistent and not easily readable results, because of the presence of large quantities of steel fibers protruding from the same cracked surfaces.

Because of this, chemical titration was performed (as per BS EN 14629:2007 or RILEM TC 178-TMC) according to a tailored methodology, suitably conceived and validated throughout this study.

The procedure consisted of drilling micro-cores (8 mm diameter) at three different positions parallel to the diameter crack and at three different distances orthogonal to it, having further care of separating the material as progressively drilled at four different equally spaced depths, down to 20 mm from the exposed surface, as shown in Figure 3. The 36 determinations obtained for each specimen allowed to "reconstruct" the chloride penetration profiles.

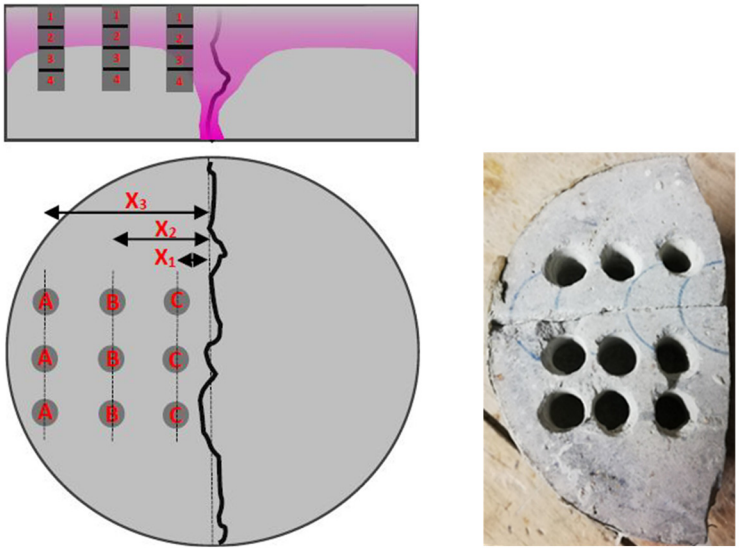

Figure 3. Schematic of core drilling for chloride titration and image of drilled split disk.

Though conscious of the theoretical non-applicability to the case of cracked concrete, the data were also used to calculate an apparent diffusion coefficient as affected by healing by fitting them through Fick's second law of diffusion, as below:

$$C(x,t) = C_0 + C_s \cdot \mathrm{erfc}\left(\frac{x}{2\cdot\sqrt{D_{app}(t)\cdot t}}\right) \quad (2)$$

where $C(x,t)$ indicates the chloride concentration at time t and depth x, C_0 and C_S are the initial and surface chloride concentration, respectively, and $D_{app}(t)$ is the apparent diffusion coefficient.

2.2.2. Self-Healing Assessment through Water Permeability Recovery

Concrete disks Ø100 × 50 mm were obtained from cylinders Ø100 × 280 mm by cutting them, after discarding the two ends (Figure 4). Five disks were obtained from each concrete cylinder. Each disk was pre-cracked by splitting test up to a residual crack width of 100 ± 50 µm after unloading, employing the same set-up as shown in Figure 1. Crack width was measured with an optical/digital microscope at three equidistant points of the length of the crack at each of the two faces of the specimen. The average crack width was thus calculated.

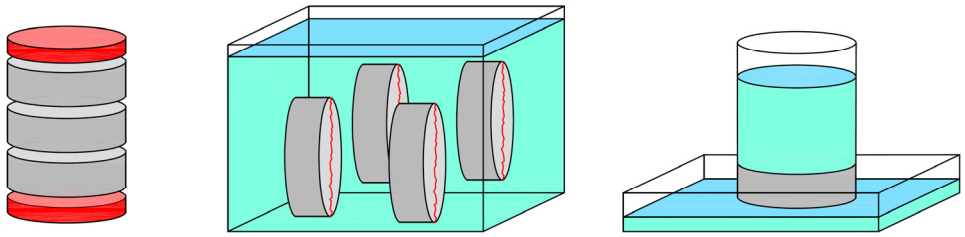

Figure 4. Concrete disks cut from cylinders and then stored in water, and schematics of the water permeability test set-up.

Before performing the water permeability test for samples healed for one and three months and up to six months, they were preconditioned for 24 h drying at 60 °C. For the permeability tests, PVC tubes of at least 550 mm height were glued on the top of the disks (Figure 4) using a resin (Sikaflex-11 FC®) that had to dry for 24 h. It is important to highlight that the resin was removed after the test. The tubes were filled with 3.5 L of tap water (beginning of filling the tube = time 0, filling time of approximately 1 min).

The water flow was monitored for 3 h by weighing the water flowing through the crack at different intervals (time = 0, 5, 10, 15, 20, 25, 30, 40, 50, 60, 80, 100, 120, 150, 180 min). From the thus measured volume of flown-through water vs. time curves, an index of permeability was calculated as the slope, K, of the stationary part of the flow curve, from which an index of permeability recovery (IPR) was calculated as an indicator of the healing capacity as follows:

$$IPR = 1 - \frac{K_t}{K_{t0}} \quad (3)$$

The permeability test was performed just after pre-cracking and after the aforementioned healing deadlines, equal to one, three, and six months.

Before performing each permeability test at a prescribed healing time, cracks were analyzed via the same image processing protocol described in Section 2.2.1.

2.2.3. Self-Healing Assessment on Pre-Cracked Thin Beams

Thin concrete slabs with a nominal thickness of 25 mm and in-plane dimensions 500 × 1000 mm^2 were cast and then cut into 20 beam specimens (100 mm wide and 500 mm long), this procedure guaranteeing a better alignment of fibers as compared to the production of single specimens.

Figure 5 shows the position of each thin beam inside the slab, also indicating the "testing purpose" to which each thin beam was destined. Table 4 shows the experimental program for bending tests on thin beams. After 60 days from casting, specimens were subjected to a four-point bending test up to a prescribed residual deformation at the bottom side, namely pre-cracking (see Table 4). The use of four-point bending test allows, in the central constant bending moment region, multiple cracking to stably develop, which is representative for materials with strain/deflection-hardening behavior.

During the test, the tensile deformation was measured at the bottom side in the region between the two loading blades by means of two displacement transducers positioned at the fixed platelets as shown in Figure 6. Flexural tests were performed in displacement control.

w/o CA 1-1	w/o CA 1-6
w/o CA 1-2	w/o CA 1-7
w/o CA 1-3	w/o CA 1-8
w/o CA 1-4	w/o CA 1-9
w/o CA 1-5	w/o CA 1-10

w/o CA 2-1	w/o CA 2-6
w/o CA 2-2	w/o CA 2-7
w/o CA 2-3	w/o CA 2-8
w/o CA 2-4	w/o CA 2-9
w/o CA 2-5	w/o CA 2-10

w CA 1-1	w CA 1-6
w CA 1-2	w CA 1-7
w CA 1-3	w CA 1-8
w CA 1-4	w CA 1-9
w CA 1-5	w CA 1-10

w CA 2-1	w CA 2-6
w CA 2-2	w CA 2-7
w CA 2-3	w CA 2-8
w CA 2-4	w CA 2-9
w CA 2-5	w CA 2-10

Cracking at 0 months	Cracking at 1 month	Cracking at 3 months	Cracking at 6 months	Self-healing	Spare specimen

Figure 5. Thin beams: experimental program and position in the four cast slabs (two per mix).

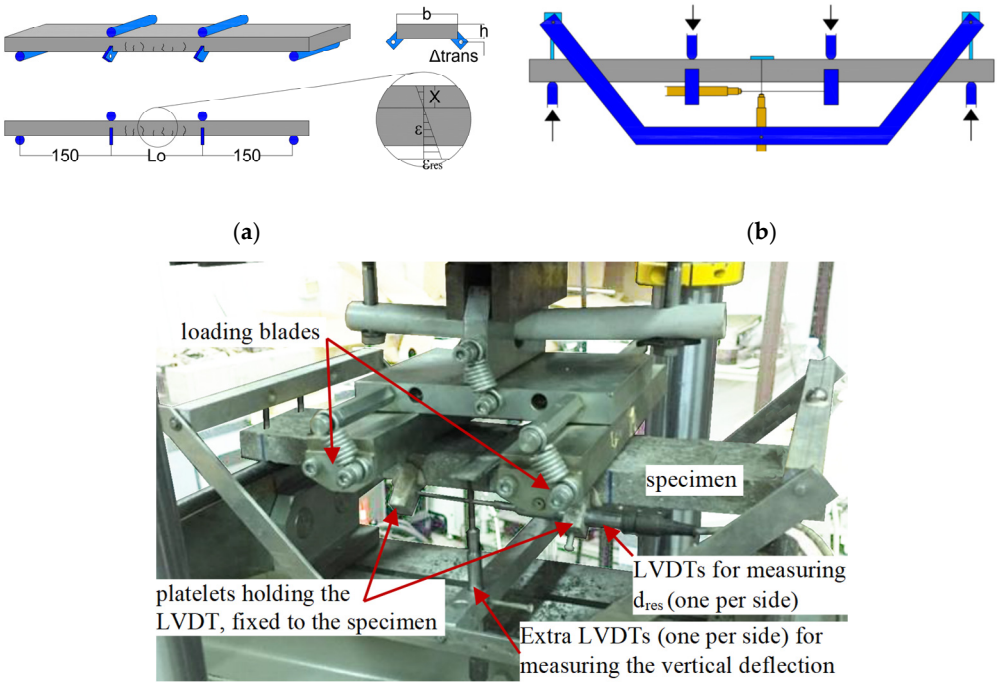

Figure 6. Schematic of the concept employed for calculation of maximum target residual displacement upon pre-cracking (**a**) and scheme (**b**) and image (**c**) of the 4-point bending test setup for pre-cracking and re-cracking.

The first step was to translate the target residual strain (at the end of the bending test) at the tension (bottom) side of the beams, ε_{res}, into a target displacement at the transduces d_{res}. The two parameters are linked by the relation:

$$d_{res} = \varepsilon_{res} \cdot L_0 \cdot (h - x + \Delta_{trans})/(h - x) \quad (4)$$

where L_0 is the base of measurement (= distance between the two loading blades = 150 mm), h is the thickness of the specimen, x is the distance between the compression side of the

specimen and the neutral axis, and Δ_{trans} is the vertical distance between the bottom face of the slab and the plane of displacement measurement.

At each cracking step (both pre-cracking and re-cracking, as it will be further explained) a residual strain (after unloading) of 1‰ should be attained. Since in the case at issue, ε_{res} was expected to be attained before unstable crack localization takes place, the value of x was reasonably assumed as 0.5 h (and consequently: $d_{res} = \varepsilon_{res} \cdot L_0 \cdot [1 + 2 \cdot \Delta_{trans}/h]$). Once the value of x was defined, the target displacement at the displacement transducers d_{res} was determined.

At the end of cracking via four-point bending, each crack at the bottom side of the specimens was identified and recorded via a digital microscope. After 1-month healing, each crack was recorded again. Afterwards, specimens were subjected again to bending in order to simulate a cyclic crack opening (namely re-cracking), by imposing a further crack opening equal to the first one, reaching a residual deformation after each cycle up to ε_{res} = 1‰, as indicated in Table 4.

The total deformation was obtained from the consecutive σ-COD cycles. To this purpose the σ-COD curves were translated along the x-axis, matching the first point of the cracking (i) with the last point of the previous cracking (i-1), as shown in Figure 7.

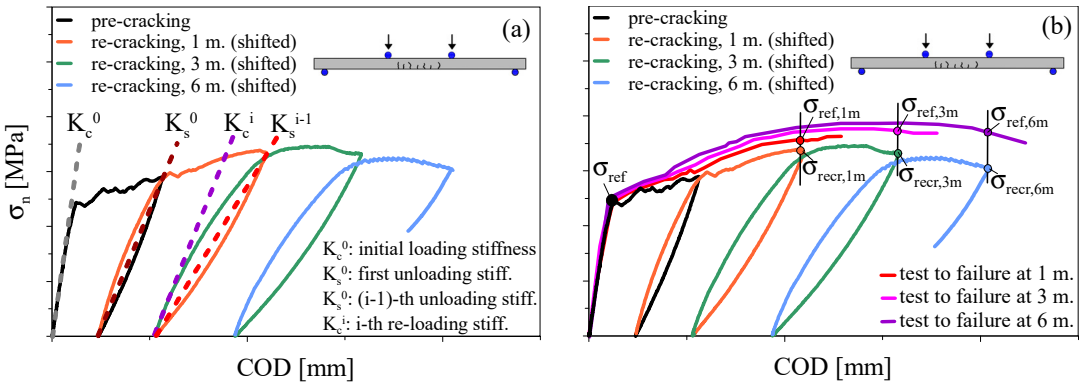

Figure 7. Evaluation of stiffness recovery index (**a**) and strength recovery index (**b**).

All cracks were recorded again by digital microscope just after cracking and then checked after further two months healing (at three months healing after first pre-cracking). Also in this case, re-cracking has to be performed. Finally, at 12 months healing after pre-cracking, cracks were recorded again by a digital microscope, and specimens were tested up to failure.

As remarked above, in Figure 7a,b, pre-cracking σ-COD law (black curve) is reported together with the re-cracking curves at 1, 3, and 12 months (respectively, orange, green, and light blue curves). The latter three curves are shifted along the COD axis of the quantity equal to the residual COD of the previous cracking stage. This curve can be compared with that of a reference specimen tested up to failure (red, magenta, and violet curves).

Re-cracking of specimens at each target interval makes it possible to evaluate the mechanical recovery from the translated σ-COD curves by means of the following indexes:

- *Index of Stiffness Recovery (ISR)* as follows:

$$ISR_0 = \frac{K_c^i - K_s^0}{K_c^0 - K_s^0} \quad (5)$$

$$ISR_{i-1} = \frac{K_c^i - K_s^{i-1}}{K_c^{i-1} - K_s^{i-1}} \quad (6)$$

where ISR_0 allows evaluation of the recovery referred to the pre-cracking cycle (first loading cycle) and ISR_{i-1} allows to evaluate the recovery referred to the previous cracking cycle (pre-cracking or re-cracking cycle). The different parameters used to determine the indexes

are the initial loading stiffness (K_c^0), the first unloading stiffness (K_s^0), the $(i-1)$th unloading stiffness (K_s^{i-1}), and the ith re-loading stiffness (K_c^i) and are indicated in Figure 7a.

- *Index of Resistance Recovery (IRR)* as follows:

$$IRR = 1 + \frac{\sigma_{recr,i} - \sigma_{ref,i}}{\sigma_{\text{ref}}} \quad (7)$$

where the different parameters are explained in Figure 7b.

The definition of the different indices has been made in such a way that a value equal to 1 indicated complete recovery of the pristine performance of the specimen in its virgin/previous state. Crack comparison was performed via the same image analysis procedure described in Section 2.2.1 and the index of crack sealing was calculated as well, with reference to the crack survey scheme in Figure 8.

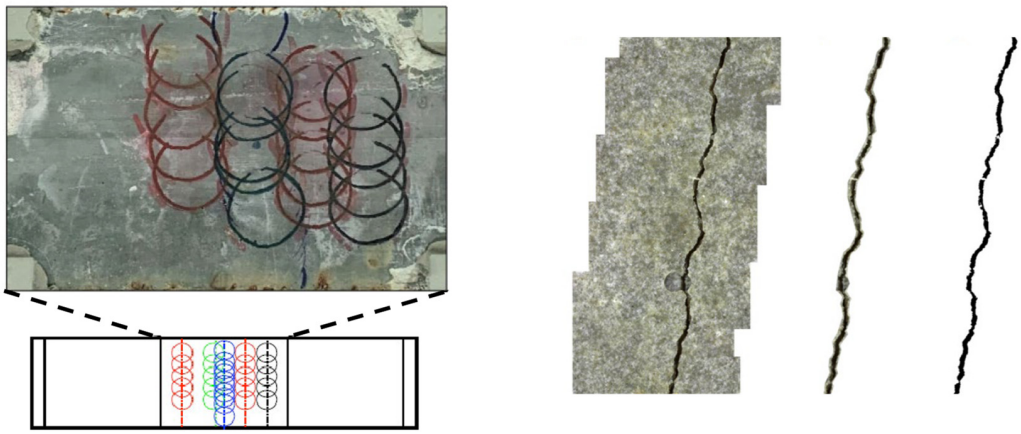

Figure 8. Crack observation using digital microscope for beam specimens.

2.3. Experimental Program Overview

Table 5 shows the overall experimental program carried out in this study, for which the following specimens have been cast:

- 15 beams 100 × 500 × 25 mm^3 without crystalline admixtures;
- 15 beams 100 × 500 × 25 mm^3 with crystalline admixtures;
- 4 cylinders (Ø100 × 280 mm^2) to be further cut in 5 disks (50 mm thick) and 9 disks (80 mm thick) for the mix without crystalline admixtures;
- 4 cylinders (Ø100 × 280 mm^2) to be further cut in 5 disks (50 mm thick) and 9 disks (80 mm thick) for the mix with crystalline admixtures.

Table 5. Overall experimental program.

Test	0 Month	1 Month	3 Months	6 or 12 Months
* Chlorides diffusion (9 specimens)	specimens 1 to 6 pre-cracked; specimens 7 to 9 un-cracked; 9 disks immersed in salt water.	specimens 1, 2, 7 broken and titrated; specimens 3 to 6 and 8, 9 kept in salt water	specimens 3, 4, 8 broken and titrated; specimens 5, 6, 9 kept in salt water.	specimens 5, 6, 9 broken and titrated.
^ Water Permeability (5 specimens)	5 specimens pre-cracked; 5 permeability test performed.	5 specimens subjected to permeability test	5 specimens subjected to permeability test.	5 specimens subjected to permeability test.
^ 4-P bending in thin beams (15 specimens)	7 specimens pre-cracked; 2 specimens tested to failure; 6 specimens uncracked with same curing of cracked ones.	7 specimens re-cracked; 2 specimens tested up to failure	7 specimens re-cracked; 2 specimens tested up to failure.	7 specimens re-cracked; 2 specimens tested up to failure.

* continuous immersion in salt water (33 g/L NaCl); ^ continuous immersion in tap water.

3. Results and Discussion

3.1. Chloride Penetration of Self-Healed Disks

The results of titration tests are shown in Figure 9, in the usual dimensionless mass percentage format, as a function of the depth parallel to the crack and for the three different distance positions orthogonal to it. Interestingly, the analysis can be performed also considering the crack sealing for the same specimens, as monitored and evaluated along the considered exposure time (Figure 10a).

After one-month exposure, in the UHPC without crystalline admixture, an immediate quite strong penetration of the chlorides throughout the crack depth is evident, with chloride content holding almost constant at 0.1% from 10 mm inward (and at 0.2% at the exposed surface, whereas a progressive decreasing trend has been measured for the mix with crystalline admixture. This can likely be the consequence of a faster crack sealing in the latter.

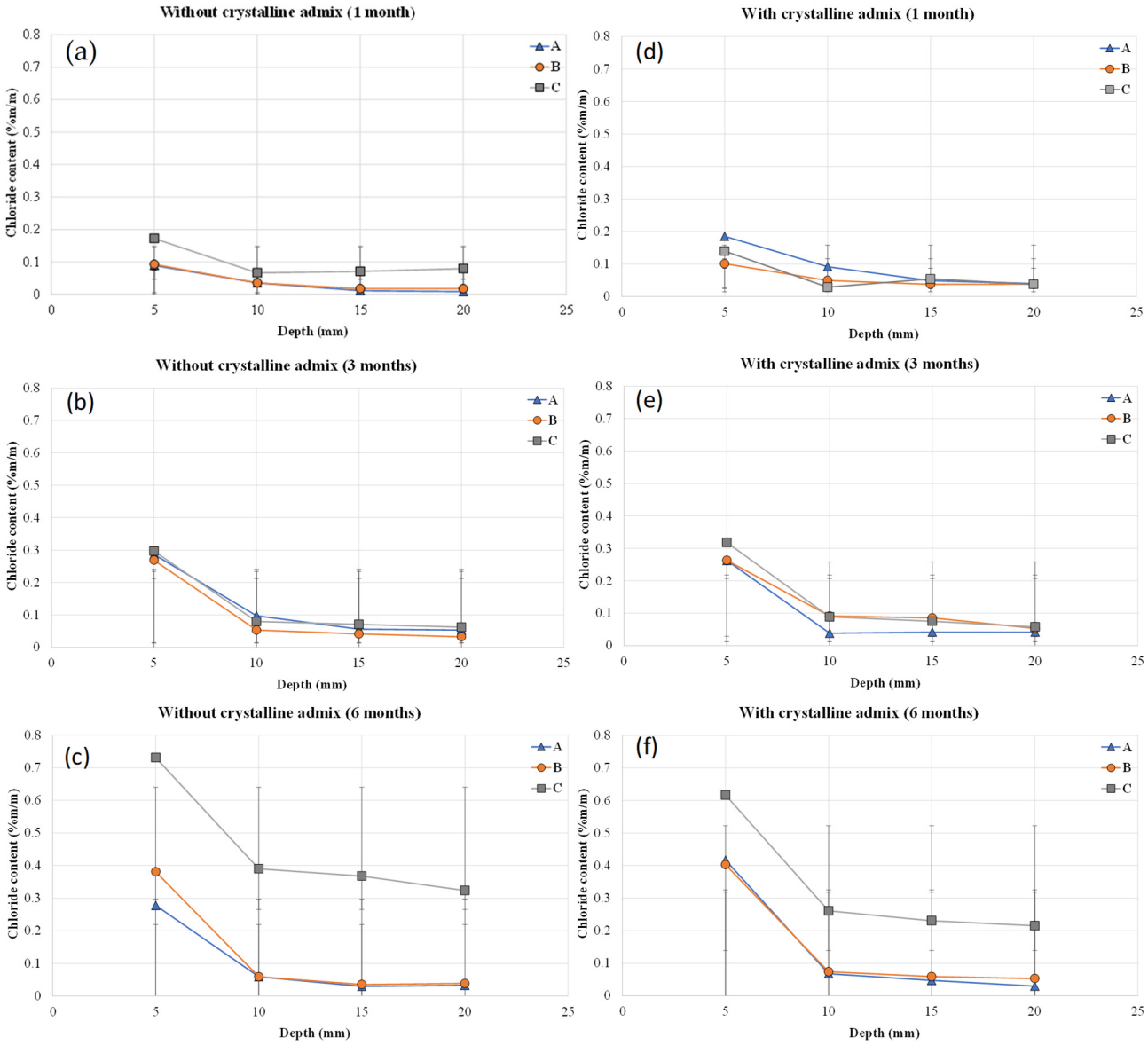

Figure 9. Chloride penetration profiles for the three exposure times as functions of depth/distance along/from the crack for specimens without (**a**–**c**) and with (**d**–**f**) crystalline admixture.

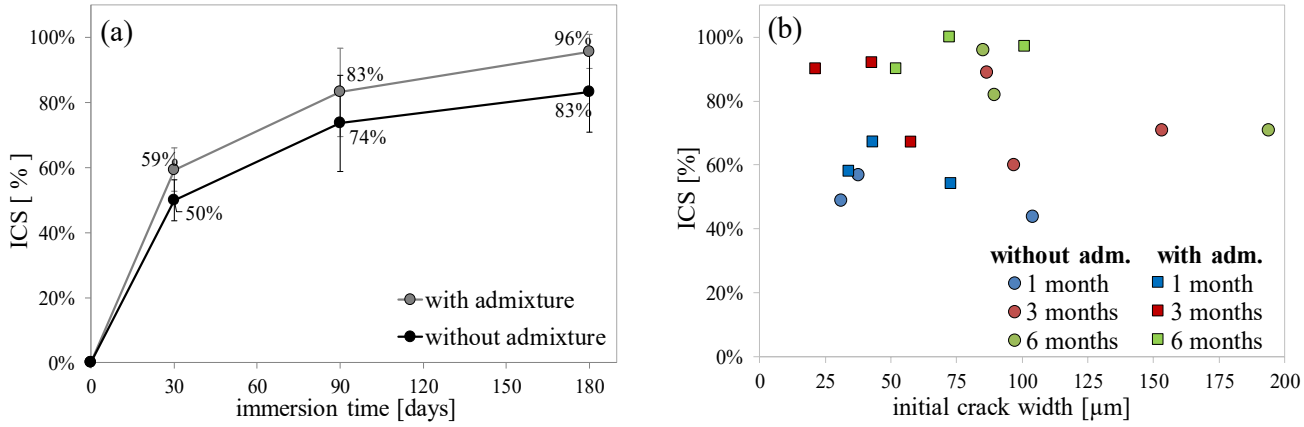

Figure 10. Index of crack sealing vs. immersion time (**a**) and vs. initial crack width (**b**) for split cracked disks with/without crystalline admixture undergoing up to six months of permanent immersion in chloride solution.

Upon three-month exposure, the chlorides continue to penetrate, but their accumulation is likely to be limited to the top 5 mm layer, no matter the orthogonal distance from the crack and no significant difference is evident between the mixes with and without the crystalline admixture, the same difference highlighted above with reference to crack sealing capacity holding.

Upon prolonged exposure, up to six months, the penetration of the chlorides along the cracked plane massively continues, in this case, the better crack sealing efficacy of the mix with the crystalline admixture being instrumental in reducing the chloride content by about 20–25% both at the exposed surface and along the crack depth, with an about threefold and twofold increase with respect to the situation measured at three months, respectively, in the mix without and with the crystalline admixture.

In both cases, the crack sealing capacity, as quantified from the index of crack sealing, was instrumental at almost "freezing" the chloride profile at positions further from the crack, in the direction orthogonal to it, to the same situation which was measured for specimens exposed up to three months. Some benefits are evident also at these positions for the mix with the crystalline admixture as opposed to the one without it.

Furthermore, it is interesting to analyze the aforementioned calculated indices of crack sealing as a function of the initial crack width, as induced through the splitting test in the disk specimens: considering the intrinsic variability of the cracking process characteristics of the test, a reasonable range of initial crack widths was obtained, variations being likely attributable to local dispersion of fibers in the specimens. A slightly faster healing in the mix with the stimulating crystalline admixture was detected, which had to capacity to almost close cracks narrower than 50 µm and 100 µm in three and six months, respectively.

From the chloride penetration profiles, extracted as above, the chloride apparent diffusion coefficient D_{app} was quantified for the different investigation healing deadlines (making reference to the three average positions shown in Figure 3) by fitting the experimental data with Fick's second law of diffusion (as shown for two cases in Figure 11). The results summarized in Table 6 show that, as expected, the diffusivity coefficient does not depend significantly on the considered position, while it is much more affected by the immersion time. It can be observed, in fact, as going from 1 to 6 months of immersion in water with NaCl, diffusivity decreases of more than one order of magnitude, showing very similar values between mixes with or without crystalline admixtures.

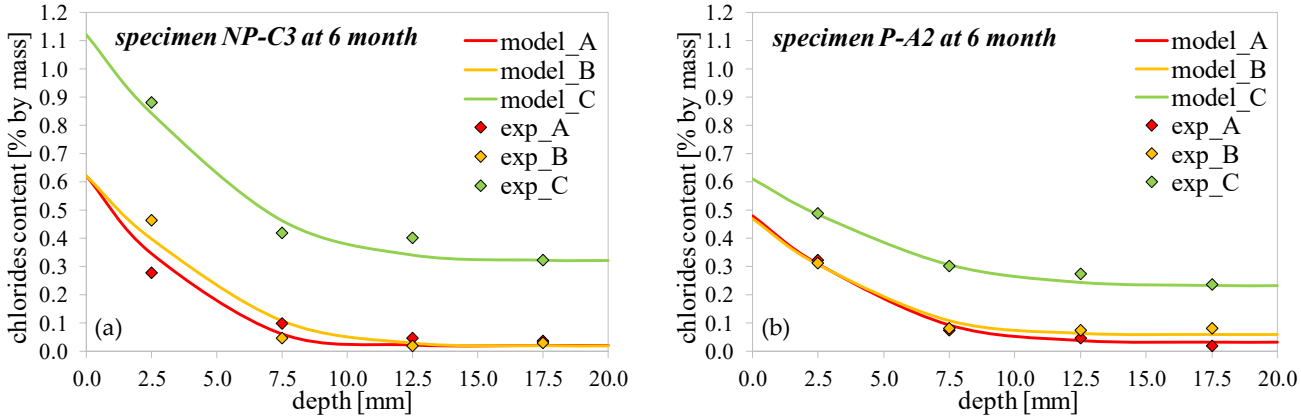

Figure 11. Examples of data fitting for a specimen without (**a**) and with (**b**) crystalline admixture after 6 months exposure.

Table 6. Apparent chloride diffusion coefficients D_{app} (10^{-12} m^2/s) for mix without and with crystalline admixtures at different healing times.

D_{app} [10^{-12} m^2/s]	Without Crystalline Admixture			With Crystalline Admixture		
Healing Time	**Pos A**	**Pos B**	**Pos C**	**Pos A**	**Pos B**	**Pos C**
1 month	21.9	22.3	20.3	23.0	26.0	22.4
3 months	5.15	3.45	4.01	5.06	5.87	5.10
6 months	1.55	1.83	1.90	1.85	2.06	1.97

On the other hand, the effect of the increased inlet of chlorides due to the presence of the crack translates into a "rigid vertical translation" of the profile towards higher values of chlorides content (Figures 9c,f and 11).

It can be observed as such "translation" is sizable at six months only and indicates the amount of chlorides entering from the cracks, this quantity being (reasonably) dependent of the crack initial opening (and following sealing thanks to self-healing phenomena) and not on disk depth. As shown in Figure 9, such quantity is quite lower in the case with crystalline admixture (about 0.2% at six months, against about 0.3% in the mix without crystalline admixture), thus proving indirectly a more pronounced sealing of the crack favored by the addition of crystalline admixture, this being consistent with the evidence of Figure 10.

3.2. Water Permeability of Self-Healed Disks

Figure 12a,b shows the indices of crack sealing and of permeability recovery for the two investigated mixtures and along the investigated healing time. The faster crack sealing promoted by the presence of the crystalline admixture, already measured above with reference to specimens undergoing immersion in chloride solution, is confirmed, also with reliable quantitative repeatability. Interestingly, the differences in terms of permeability recovery are scant, likely due to the significance of the test set-up when flow through very narrow cracks and with a limited water pressure overhead is considered, already widely assessed in the literature [38,39].

Similar to what was carried out for previously investigated chloride penetration, the index of crack sealing has been correlated to the initial crack width (Figure 13). The range of crack widths is comparable to the one obtained in split cylinders employed for chloride penetration tests. The aforementioned correlation also confirms the previous findings, with reference to the faster sealing capacity and higher effectiveness, even for larger crack width, guaranteed by the crystalline admixture as well as to the range of crack widths for which the same admixture is able to guarantee complete sealing of the cracks upon longer-term exposure [37].

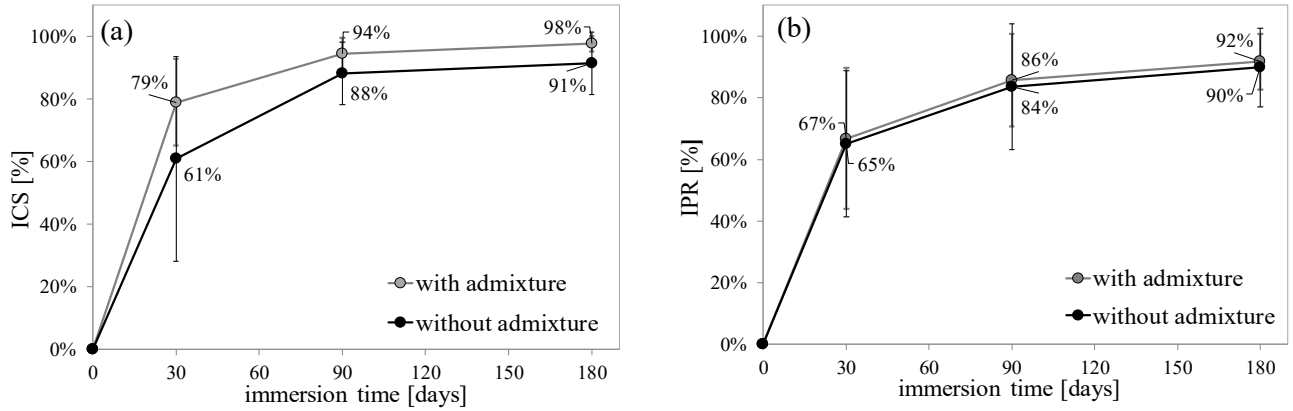

Figure 12. Index of crack sealing (**a**) and of permeability recovery (**b**) for split-cracked disks undergoing up to six months permanent immersion in tap water.

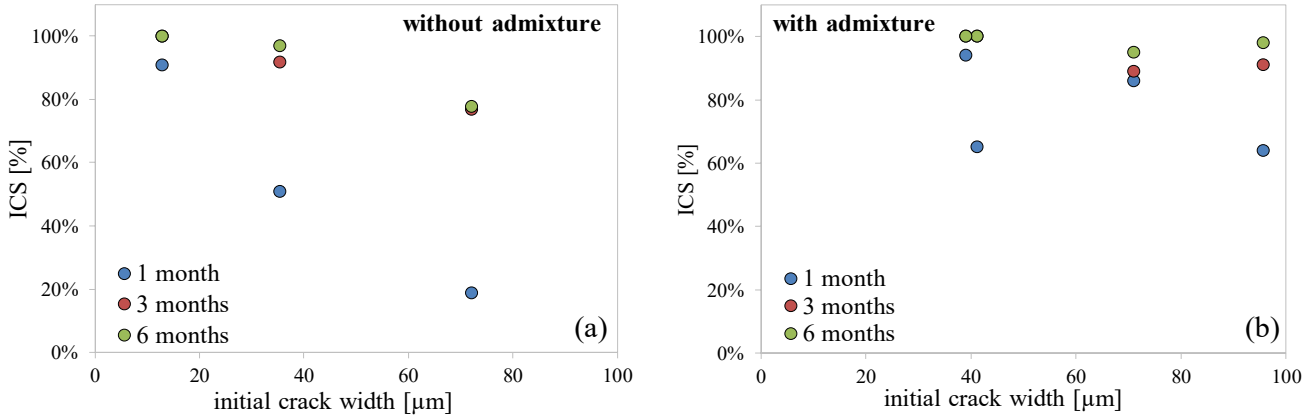

Figure 13. Index of crack sealing vs. initial crack width for split-cracked disks permanently immersed up to six months in tap water, for the mix without (**a**) or with (**b**) crystalline admixture.

3.3. Comparative Analysis of Crack Sealing Capacity in Tap Water and Chloride Solution

Figure 14 compares for the two investigated mixes and for both exposure conditions so far considered (i.e., immersion in tap and chloride water) as a function of the initial crack width, healing duration having been further considered as an experimental variable.

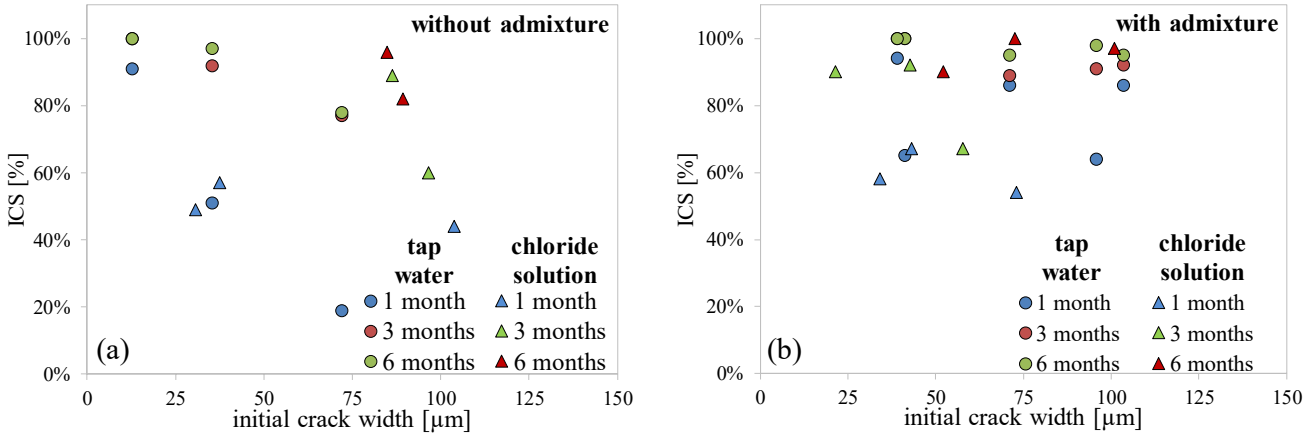

Figure 14. Comparison of indices of crack sealing for mixes without (**a**) or with (**b**) crystalline admixture in the case of immersion in tap water and chloride aqueous solution.

It can be clearly observed that for the reference a better crack sealing capacity has been obtained when specimens were immersed in the chloride aqueous solution, as likely

due to the chloride binding capacity of the matrix, which may result in additional precipitates sealing the crack volume. In the case of the mix containing the healing-stimulating crystalline admixture, the difference is less evident, likely due to the already almost complete sealing of the cracks obtained already after three months of immersion in all the investigated specimens.

3.4. Mechanical Recovery of Self-Healed Thin Beams

The use of a four-point bending test set-up allows multiple cracking to develop in the central constant bending moment region of each specimen. Tensile deformation was measured at the bottom side between the supports by means of displacement transducers across the whole central zone. For the determination of the crack sealing capacity, the area of each crack was determined (Figure 15), highlighting, on a global trend, no significant difference between the two mixes.

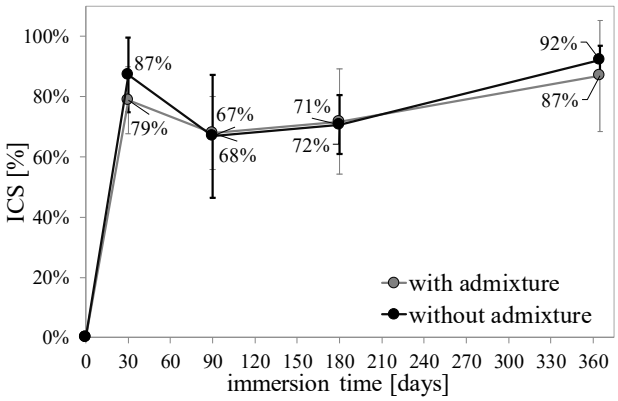

Figure 15. Index of crack sealing for thin beam specimens tested in 4-point bending.

For a deeper analysis, Figure 16 shows the crack width distribution, plotting the number of cracks versus crack width (organized in crack widths ranges of 10 μm) for different observation periods:

- time 0: the start of the first observation period (a);
- the end of the first observation period, i.e., after one month healing (b);
- the start of the second observation period, after first re-cracking after one month healing (c);
- the end of the second observation period, which is after three months healing (d).

In the third observation period, re-cracking at six months was not possible (due to restrictions imposed by the COVID-19 pandemic) and only an intermediate observation was performed after six months healing, before the final observation performed after twelve months healing, which immediately preceded the final failure tests. Crack sealing at both the aforesaid deadlines was nearly complete for almost all the cracks and data plotting in the form of histograms is deemed not significant.

Data in Figure 16 show that, for an almost equal total number of observed cracks, specimens with crystalline admixture show, after pre- and re-cracking events, a higher crack frequency for wider crack widths. Nonetheless, after the scheduled healing periods, the crack frequency distribution tends to be shifted towards the narrower widths (almost all the observed cracks are below 20 μm).

Furthermore, and even more interestingly, while the number of cracks falling in the narrowest 0–10 μm width range decreases for the mix without crystalline admixture for cracking and healing cycles, it holds constant in the case of the mix with crystalline admixture, this signifying a stronger persistence of the healing capacity upon repeated events.

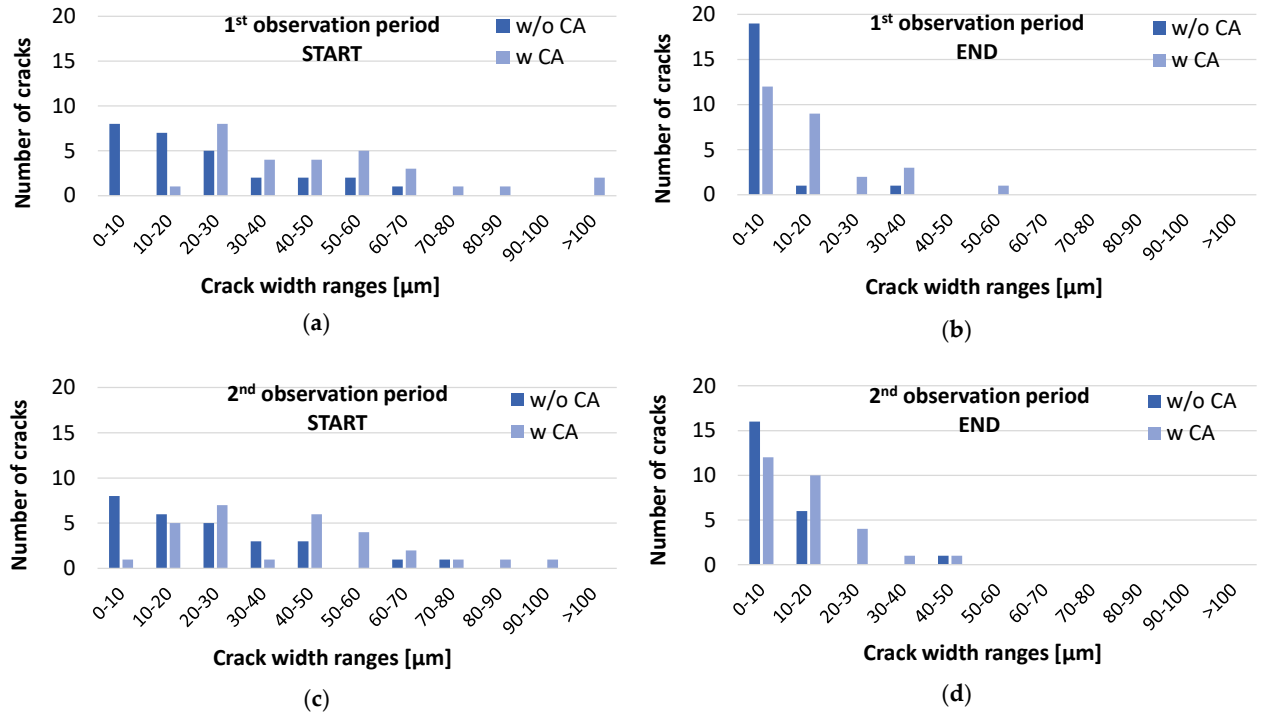

Figure 16. Crack width distribution: (**a**) time 0: start of the first observation period, (**b**) end of the first observation period, (**c**) start of the second observation period, and (**d**) end of the second observation period.

This better capacity of the mix with crystalline admixture to continue sealing the cracks upon prolonged exposures is also confirmed by the data as plotted in Figure 17, highlighting, through a sort of "*crack-width healability threshold*", as the mixture containing the crystalline admixture (acting as crack sealing and self-healing stimulator) is able to guarantee a given crack sealing capacity for crack widths about twice as much larger than in the companion admixture-less mix.

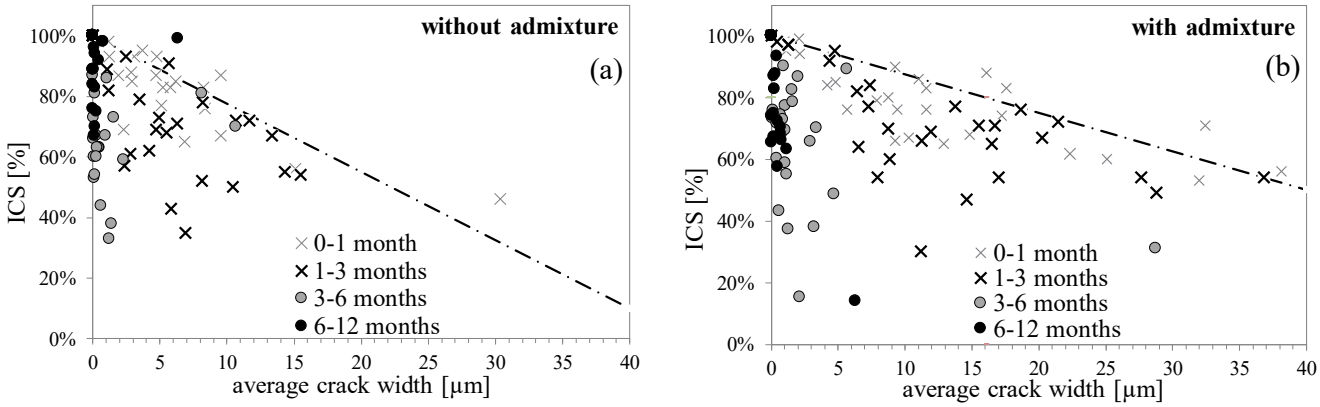

Figure 17. Crack sealing index vs. crack width: *crack-width healability thresholds* for UHPFRCC mixes without (**a**) and with (**b**) crystalline admixture as crack sealing/self-healing stimulator.

Mechanical recovery related to self-healing was evaluated on pre-cracked and re-cracked thin beams by calculating the indexes defined in Section 2.2.1 for each specimen. The average values have been plotted in Figure 18a–c and correlated to the initial crack width in Figure 18d–f.

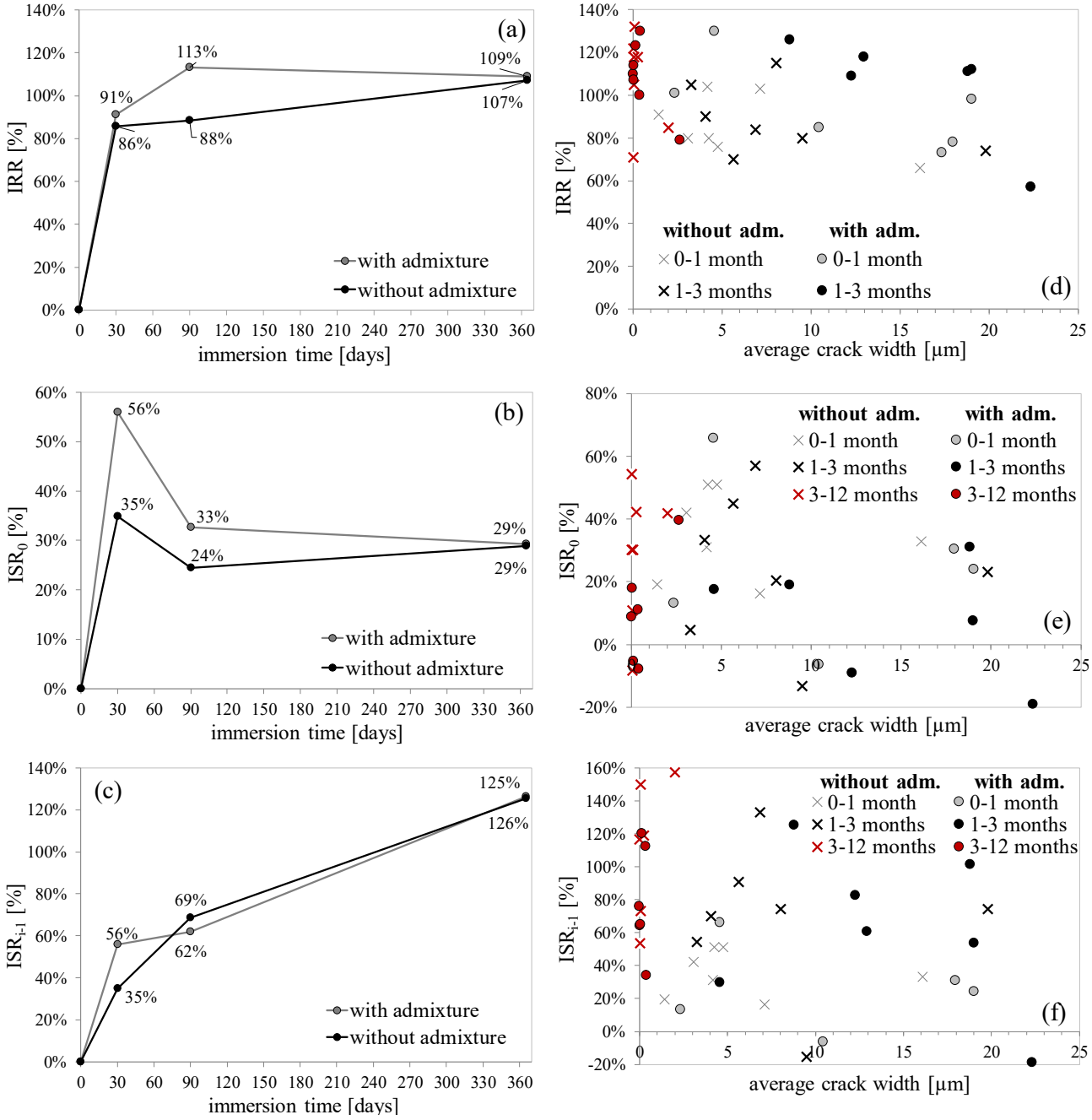

Figure 18. Indices of strength (**a**) and stiffness recovery (**b**,**c**) vs. healing time and indices of strength (**d**) and stiffness recovery (**e**,**f**) vs. average initial crack width.

The effects of faster healing promoted by the crystalline admixture are evident also on the recovery trends of the flexural strength and stiffness at shorter exposure times equal to one and three months, while after prolonged exposure these differences tend to level off, likely due to the peculiar composition of the mixes which both feature high binder content and lower water binder ratio and hence high conduciveness to autogenous healing. Interestingly, this capacity continues to be guaranteed, also upon successive re-cracking (Figure 18c,f) up to quite long exposure times, this being a very important aspect to be taken into account in real applications.

3.5. Correlation between Indices of Mechanical Recovery and Index of Crack Sealing

The indices of mechanical recovery can be interestingly correlated to the index of crack sealing, providing insightful information not only on the role of the healing stimulating

crystalline admixture, but also on the causes of the measured recovery of mechanical properties (Figure 19).

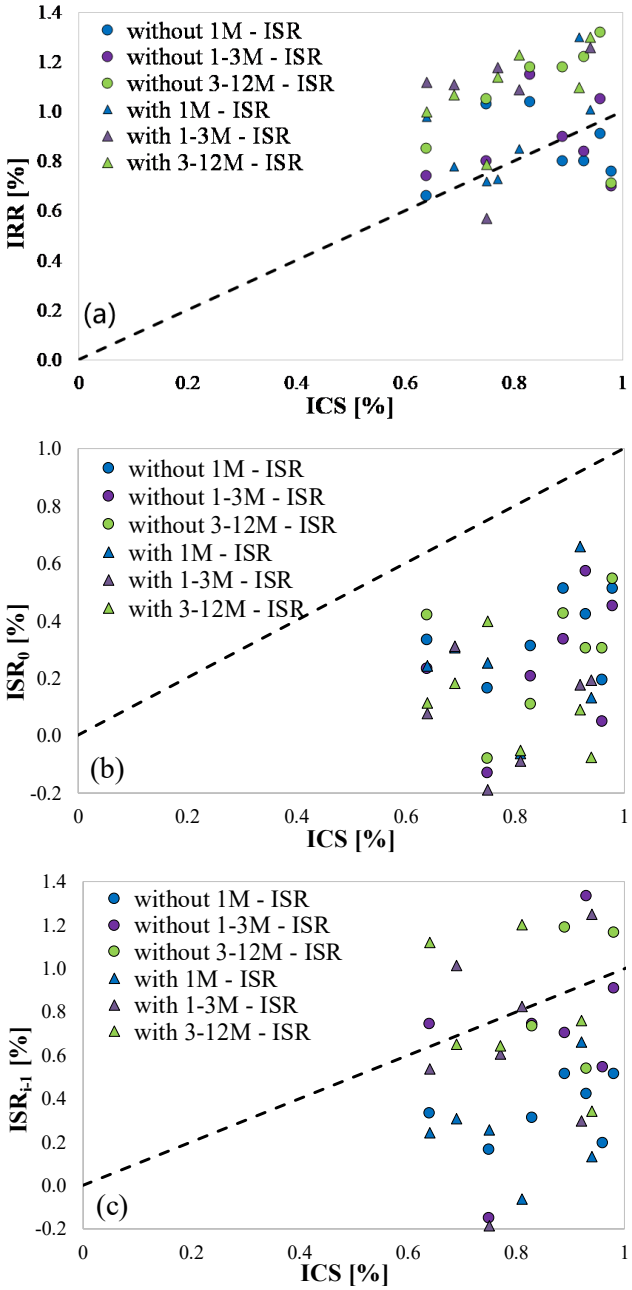

Figure 19. Indices of strength (**a**) and stiffness recovery (**b**,**c**) vs. index of crack sealing.

Though the expected scattering of the results, it can be clearly observed that the performance recovery in the mix with crystalline admixture is always consistently higher than for the mix without it for the same level of crack closure. This would lead to consistently hypothesize that the measured and calculated recovery of mechanical performance is attributable not only to a reconstruction of the physical through-crack continuity of the cementitious matrix, but also to the positive benefit induced by the healing at the level of fiber–matrix interface, as widely verified in the literature [40]. This last effect is likely to be better promoted by the crystalline admixture, also through its well-assessed pore refinement and matrix densification effect [41–43].

The significance of the different indices of recovery of mechanical performance can be appropriately interpreted in the framework of a durability-based design approach, as the

capability of the material to retain, in the intended structural service scenario encompassing environmental exposure and cracking state, its mechanical performance, and hence its design parameters, which govern the assessment of the ultimate and serviceability limit state structural capacity.

In this respect, data plotted in the graphs in Figure 19 also highlight the role of "*crack healability*", i.e., the effective capacity of the material to self-seal the cracks as a function of their initial opening, can be assumed as a parameter discriminating the effects of self-healing on the mechanical performance and hence on the structural design parameters.

Similarly, the correlation highlighted in Sections 3.1 and 3.2 between the crack sealing and the recovery of durability parameters will provide complementary information for a thorough assessment on the effects of the latter on the same persistence of mechanical properties and design parameters, in a holistic vision to a durability–performance-based structural design.

4. Conclusions

In this paper, the influence of crack self-sealing on the recovery of durability (chloride penetration resistance and water permeability) and mechanical properties (flexural strength and stiffness) of Ultra-High Performance Fiber-Reinforced Concrete has been investigated. Autogenous healing and engineered healing promoted with the addition of crystalline admixtures have been considered. To this purpose, dedicated experimental methodologies have been employed and healing-induced performance recovery has been quantified by means of suitably defined indices which also allowed a cross-comparison of results among different tests.

The cross-wise analysis of data obtained from different tests provided consistent results which is the first proof of the reliability of the performed study, on whose basis the following conclusions can be drawn:

- A dedicated experimental methodology has been developed and validated to study the chloride penetration resistance in mixes characterized by a high content of metallic fibers, which could jeopardize the readability of the simple silver nitrate test. The proposed methodology, based on multi-position and multi-depth core-drilling has allowed reconstructing of the three-dimensional characteristics of the chloride penetration both parallel and orthogonal to an existing crack, as also affected by self-healing.
- Crack sealing can significantly delay the chloride penetration in the direction orthogonal to the crack; the effects of crystalline admixture on chloride penetration tend to become more significant at longer exposure times and for chloride penetration parallel to the crack, blocking the chloride penetration to the outmost exposed layers (5 mm) and also significantly reducing their accumulation in the aforesaid region.
- As long as narrow cracks are produced in UHPFRC specimens and are progressively healed along exposure times, the reliability of permeability tests, with limited water-head, to verify the effects of crack sealing on the recovery of transport properties can be questioned; results herein obtained have shown that below a certain crack width (few tens of microns), an almost complete recovery of impermeability is apparently measured with the proposed test set-up, independently of both the crack width and the sealing efficacy.
- Being both investigated mixes, without and with the crystalline admixture, characterized by a composition which is highly conducive to autogenous self-healing, the effect of the latter on the stimulation of healing reactions is evident in the promotion of a faster closure of the cracks as well as in the capacity of guaranteeing a better self-sealing for larger crack widths. This is likely to be confirmed by the results obtained from the whole set of tests herein performed.
- The recovery of mechanical performance in the mix with crystalline admixture is consistently always higher than for the mix without it, for the same level of crack closure. This would lead to consistently hypothesize that the measured and calculated recovery of mechanical performance is attributable not only to a reconstruction of the

physical through-crack continuity of the cementitious matrix, but also to the positive benefit coming from the healing at the level of fiber–matrix interface, an effect which the crystalline admixture is likely to better promote, also through its well-assessed pore refinement and matrix densification effect.

The aforesaid findings can pave the way towards the definition of a durability-based design approach for the investigated category of cement-based materials, where the evolution of the material properties, as also benefiting from self-healing, can be incorporated into life-cycle-based structural design algorithms to plan maintenance interventions. This could be carried out to also assess the benefits of self-healing technologies in delaying such interventions and reducing their frequency, and predict the evolution of the structural performance over time and quantify the (in case residual) structural service life, defined as the time when the structural performance will no longer be able to meet the demand.

The proposed correlation between the indices of recovery of durability and mechanical performance and the index of crack sealing, together with the concept of "*crack-width healability threshold*", can be usefully exploited to incorporate the self-healing concepts into code-based design approaches, as above, also through the elaboration and use of suitably defined meta-analysis algorithms, which, managing and processing big amount of data from the available literature, will also be able to provide confidence ranges for the proposed correlations.

Author Contributions: Conceptualization, writing—original draft preparation and methodology, E.C., F.L.M. and L.F.; validation, investigation, data curation and visualization, E.C., F.L.M., M.M. and A.S.; supervision, project administration and funding acquisition, L.F. All authors have read and agreed to the published version of the manuscript.

Funding: The research activity reported in this paper has been performed in the framework of the ReSHEALience project (Rethinking coastal defence and Green-energy Service infrastructures through enHancEd-durAbiLity high-performance cement-based materials) which has received funding from the European Union's Horizon 2020 research and innovation program under grant agreement No 760824 (www.uhdc.eu, accessed on 6 October 2021). The proposed methodology is going to be implemented in a round-robin testing activity, also supported by COST Action CA 15202 "SARCOS" (http://www.sarcos.enq.cam.ac.uk, accessed on 6 October 2021).

Institutional Review Board Statement: Not applicable.

Informed Consent Statement: Not applicable.

Data Availability Statement: Data will be made available through the website www.uhdc.eu, accessed on 6 October 2021.

Acknowledgments: The research activity reported in this paper has been performed in the framework of the ReSHEALience project (Rethinking coastal defence and Green-energy Service infrastructures through enHancEd-durAbiLity high-performance cement-based materials) which has received funding from the European Union's Horizon 2020 research and innovation program under grant agreement No 760824 (www.uhdc.eu, accessed on 6 October 2021). The proposed methodology is going to be implemented in a round-robin testing activity, also supported by COST Action CA 15202 "SARCOS" (http://www.sarcos.enq.cam.ac.uk accessed on 6 October 2021).

Conflicts of Interest: The authors declare no conflict of interest.

References

1. Ferrara, L.; Van Mullem, T.; Alonso, M.C.; Antonaci, P.; Borg, R.P.; Cuenca, E.; Jefferson, A.; Ng, P.; Peled, A.; Roig-Flores, M.; et al. Experimental characterization of the self-healing capacity of cement based materials and its effects on the material performance: A state of the art report by COST Action SARCOS WG2. *Constr. Build. Mater.* **2018**, *167*, 115–142. [CrossRef]
2. De Belie, N.; Gruyaert, E.; Al-Tabbaa, A.; Antonaci, P.; Baera, C.; Bajare, D.; Darquennes, A.; Davies, R.; Ferrara, L.; Jefferson, T.; et al. A Review of Self-Healing Concrete for Damage Management of Structures. *Adv. Mater. Interfaces* **2018**, *5*. [CrossRef]
3. Jefferson, T.; Javierre, E.; Freeman, B.; Zaoui, A.; Koenders, E.; Ferrara, L. Research Progress on Numerical Models for Self-Healing Cementitious Materials. *Adv. Mater. Interfaces* **2018**, *5*, 1701378. [CrossRef]

4. Hilloulin, B.; Hilloulin, D.; Grondin, F.; Loukili, A.; De Belie, N. Mechanical regains due to self-healing in cementitious materials: Experimental measurements and micro-mechanical model. *Cem. Concr. Res.* **2016**, *80*, 21–32. [CrossRef]
5. Al-Obaidi, S.; Bamonte, P.; Luchini, M.; Mazzantini, I.; Ferrara, L. Durability-based design of structures made with UHP/UHDC in extremely aggressive scenarios: Application to a geothermal water basin case study. *Infrastructures* **2020**, *5*, 102. [CrossRef]
6. Escoffres, P.; Desmettre, C.; Charron, J.-P. Effect of a crystalline admixture on the self-healing capability of high-performance fiber reinforced concretes in service conditions. *Constr. Build. Mater.* **2018**, *173*, 763–774. [CrossRef]
7. di Summa, D.; Snoeck, D.; Tenorio Filho, J.R.; Van den Heede, P.; Van Vielrberghe, S.; Ferrara, L.; de Belie, N. Sustainability and economic viability of self-healing concrete containing Superabsorbent polymers. In Proceedings of the RILEM 75th Annual Week, International Conference on Advances in Sustainable Construction Materials and Structures, Merida, Mexico, 31 August–2 September 2021.
8. Jacobsen, S.; Marchand, J.; Boisvert, L. Effect of cracking and healing on chloride transport in OPC concrete. *Cem. Concr. Res.* **1996**, *26*, 869–881. [CrossRef]
9. Şahmaran, M. Effect of flexure induced transverse crack and self-healing on chloride diffusivity of reinforced mortar. *J. Mater. Sci.* **2007**, *42*, 9131–9136. [CrossRef]
10. Ismail, M.; Toumi, A.; Francois, R.; Gagné, R. Effect of crack opening on the local diffusion of chloride in cracked mortar samples. *Cem. Concr. Res.* **2008**, *38*, 1106–1111. [CrossRef]
11. Maes, M.; De Belie, N. Resistance of concrete and mortar against combined attack of chloride and sodium sulphate. *Cem. Concr. Compos.* **2014**, *53*, 59–72. [CrossRef]
12. Maes, M.; Snoeck, D.; De Belie, N. Chloride penetration in cracked mortar and the influence of autogenous crack healing. *Constr. Build. Mater.* **2016**, *115*, 114–124. [CrossRef]
13. Jiang, J.; Zheng, X.; Wu, S.; Liu, Z.; Zheng, Q. Nondestructive experimental characterization and numerical simulation on self-healing and chloride ion transport in cracked ultra-high performance concrete. *Constr. Build. Mater.* **2019**, *198*, 696–709. [CrossRef]
14. Palin, D.; Jonkers, H.; Wiktor, V. Autogenous healing of sea-water exposed mortar: Quantification through a simple and rapid permeability test. *Cem. Concr. Res.* **2016**, *84*, 1–7. [CrossRef]
15. Savija, B.; Schlangen, E. Autogeneous healing and chloride ingress in cracked concrete. *Heron* **2016**, *61*, 15–32.
16. Darquennes, A.; Olivier, K.; Benboudjema, F.; Gagné, R. Self-healing at early-age, a way to improve the chloride resistance of blast-furnace slag cementitious materials. *Constr. Build. Mater.* **2016**, *113*, 1017–1028. [CrossRef]
17. Van den Heede, P.; Maes, M.; De Belie, N. Influence of active crack width control on the chloride penetration resistance and global warming potential of slabs made with fly ash+silica fume concrete. *Constr. Build. Mater.* **2014**, *67*, 74–80. [CrossRef]
18. Xue, C.; Li, W.; Luo, Z.; Wang, K.; Castel, A. Effect of chloride ingress on self-healing recovery of smart cementitious composite incorporating crystalline admixture and MgO expansive agent. *Cem. Concr. Res.* **2021**, *139*, 106252. [CrossRef]
19. Borg, R.P.; Cuenca, E.; Brac, E.M.G.; Ferrara, L. Crack sealing capacity in chloride-rich environments of mortars containing different cement substitutes and crystalline admixtures. *J. Sustain. Cem. Mater.* **2018**, *7*, 141–159. [CrossRef]
20. Cuenca, E.; Rigamonti, S.; Gastaldo Brac, E.; Ferrara, L. Improving resistance of cracked concrete to chloride diffusion through "healing stimulating" crystalline admixtures. *ASCE J. Mater. Civ. Eng.* **2021**, *33*, 1–14. [CrossRef]
21. Ling, H.; Chunxiang, Q. Effects of self-healing cracks in bacterial concrete on the transmission of chloride during electromigration. *Constr. Build. Mater.* **2017**, *144*, 406–411. [CrossRef]
22. Maes, M.; Van Tittelboom, K.; De Belie, N. The efficiency of self-healing cementitious materials by means of encapsulated polyurethane in chloride containing environments. *Constr. Build. Mater.* **2014**, *71*, 528–537. [CrossRef]
23. Van Belleghem, B.; Sylvia, K.; Van den Heede, P.; Van Tittelboom, K.; der Belie, N. Chloride induced reinforcement corrosion behavior in self-healing concrete with encapsulated polyurethane. *Cem. Concr. Res.* **2018**, *113*, 130–139. [CrossRef]
24. Li, M.; Li, V. Cracking and healing of Engineered Cementitious Composites under chloride environment. *ACI Mater. J.* **2011**, *108*, 333–340. [CrossRef]
25. Van Belleghem, B.; Heede, P.V.D.; Van Tittelboom, K.; De Belie, N. Quantification of the Service Life Extension and Environmental Benefit of Chloride Exposed Self-Healing Concrete. *Materials* **2016**, *10*, 5. [CrossRef]
26. Gupta, S.; Al-Obaidi, S.; Ferrara, L. Meta-Analysis and Machine Learning Models to Optimize the Efficiency of Self-Healing Capacity of Cementitious Material. *Materials* **2021**, *14*, 4437. [CrossRef]
27. Cuenca, E.; Criado, M.; Gimenez, M.; Alonso, M.C.; Ferrara, L. Durability of ultra-high performance fiber reinforced cementitious composites exposed to chemically aggressive environments: Up-grading to ultra-high durability concrete through nano-constituents. *ASCE J. Mater. Civ. Eng.* **2021**, submitted for publication.
28. Li, V.C.; Wu, H.-C. Conditions for Pseudo Strain-Hardening in Fiber Reinforced Brittle Matrix Composites. *Appl. Mech. Rev.* **1992**, *45*, 390–398. [CrossRef]
29. Li, V.; Stang, H.; Krenchel, H. Micromechanics of crack bridging in fibre-reinforced concrete. *Mater. Struct.* **1993**, *26*, 486–494. [CrossRef]
30. Li, V.C. On engineered cementitious composites. A review of the material and its applications. *J. Adv. Concr. Technol.* **2003**, *1*, 215–230. [CrossRef]
31. Lo Monte, F.; Ferrara, L. Tensile behaviour identification in Ultra-High Performance Fibre Reinforced Cementitious Composites: Indirect tension tests and back analysis of flexural test results. *Mater. Struct.* **2020**, *53*, 1–12. [CrossRef]

32. Al-Obaidi, S.; Bamonte, P.; Animato, F.; Lo Monte, F.; Mazzantini, I.; Luchini, M.; Scalari, S.; Ferrara, L. Innovative Design Concept of Cooling Water Tanks/Basins in Geothermal Power Plants Using Ultra-High-Performance Fiber-Reinforced Concrete with Enhanced Durability. *Sustainability* **2021**, *13*, 9826. [CrossRef]
33. Lo Monte, F.; Ferrara, L. Self-healing characterization of UHPFRCC with crystalline admixture: Experimental assessment via multi-test/multi-parameter approach. *Constr. Build. Mater.* **2021**, *283*, 122579. [CrossRef]
34. Ferrara, L.; Krelani, V.; Carsana, M. A fracture testing based approach to assess crack healing of concrete with and without crystalline admixtures. *Constr. Build. Mater.* **2014**, *68*, 515–531. [CrossRef]
35. Ferrara, L.; Krelani, V.; Moretti, F. On the use of crystalline admixtures in cement based construction materials: From porosity reducers to promoters of self healing. *Smart Mater. Struct.* **2016**, *25*, 084002. [CrossRef]
36. Cuenca, E.; Tejedor, A.; Ferrara, L. A methodology to assess crack-sealing effectiveness of crystalline admixtures under repeated cracking-healing cycles. *Constr. Build. Mater.* **2018**, *179*, 619–632. [CrossRef]
37. Cuenca, E.; D'Ambrosio, L.; Lizunov, D.; Tretjakov, A.; Volobujeva, O.; Ferrara, L. Mechanical properties and self-healing capacity of Ultra High Performance Fibre Reinforced Concrete with alumina nano-fibres: Tailoring Ultra High Durability Concrete for aggressive exposure scenarios. *Cem. Concr. Compos.* **2021**, *118*, 103956. [CrossRef]
38. Roig-Flores, M.; Moscato, S.; Serna, P.; Ferrara, L. Self-healing capability of concrete with crystalline admixtures in different environments. *Constr. Build. Mater.* **2015**, *86*, 1–11. [CrossRef]
39. Roig-Flores, M.; Pirritano, F.; Serna, P.; Ferrara, L. Effect of crystalline admixtures on the self-healing capability of early-age concrete studied by means of permeability and crack closing tests. *Constr. Build. Mater.* **2016**, *114*, 447–457. [CrossRef]
40. Qiu, J.; He, S.; Wang, Q.; Su, H.; Yang, E.H. Autogenous healing of fibre/matrix interface and its enhancement of interface between micro polymeric fiber and hydraulic cement matrix. *Cem. Concr. Res.* **2019**, *124*, 105830. [CrossRef]
41. Oliveira, A.D.S.; Gomes, O.D.F.M.; Ferrara, L.; Fairbairn, E.D.M.R.; Filho, R.D.T. An overview of a twofold effect of crystalline admixtures in cement-based materials: From permeability-reducers to self-healing stimulators. *J. Build. Eng.* **2021**, *41*, 102400. [CrossRef]
42. Li, G.; Huang, X.; Lin, J.; Jiang, X.; Zhang, X. Activated chemicals of cementitious capillary crystalline waterproofing materials and their self-healing behaviour. *Constr. Build. Mater.* **2018**, *200*, 36–45. [CrossRef]
43. Zhang, Y.; Zuo, L.; Yang, J.; Cai, X.; Zhao, Y.; Zeng, X. Effect of cementitious capillary crystalline waterproofing coating on the gas permeability of mortar. *Struct. Concr.* **2019**, *20*, 1763–1770. [CrossRef]